Thirty-seven year mass balance of Devon Ice Cap, Nunavut, Canada, determined by shallow ice coring and melt modeling

Douglas Mair
Department of Geography and Environment, University of Aberdeen, Aberdeen, UK

David Burgess and Martin Sharp
Department of Earth and Atmospheric Sciences, University of Alberta, Edmonton, Alberta, Canada

Received 8 October 2003; revised 18 November 2004; accepted 30 November 2004; published 22 February 2005.

[1] In April–May 2000, eight boreholes were drilled to ~15–20 m depth on the Devon Ice Cap. ^{137}Cs γ activity profiles of each borehole showed a peak count rate at depth that is associated with fallout from atmospheric thermonuclear weapons testing in 1963. Snow, firn, and ice densities were measured at each core site and were used to estimate the average pattern of mass balance across the accumulation zone of the ice cap over the period 1963–2000. The average mass balance across the entire ice cap for the period 1960–2000 was also estimated using a degree-day model driven by data derived from on-ice temperature sensors and long-term measurements at Resolute Bay. Best fitting degree-day factors were determined for different sectors of the ice cap by comparing model output with repeated annual mass balance measurements made along two transects (Koerner, 1970). The results suggest that the ice cap has lost ~1.6 km^3 water per year, equivalent to a mean net mass balance of approximately −0.13 m We a^{-1}. Estimates of the mean mass balance for individual drainage basins reveal regions of positive and negative mass balance that are consistent with remotely sensed observations of advancing and retreating ice cap margins, respectively.

Citation: Mair, D., D. Burgess, and M. Sharp (2005), Thirty-seven year mass balance of Devon Ice Cap, Nunavut, Canada, determined by shallow ice coring and melt modeling, *J. Geophys. Res.*, *110*, F01011, doi:10.1029/2003JF000099.

1. Introduction

[2] Global climate models consistently predict that anthropogenic climate warming will be strongest at high northern latitudes [*Intergovernmental Panel on Climate Change*, 2001; *Mitchell et al.*, 1995]. Such a change in climate may cause significant changes in the mass and geometry of high Arctic ice masses, and there is evidence that such changes may be underway [e.g., *Dowdeswell et al.*, 1997; *Paterson and Reeh*, 2001; *Burgess and Sharp*, 2004]. To help elucidate the causes of these changes, it is necessary to gather baseline information on the mass balance of whole ice caps. The ice caps of the Canadian high Arctic are ideally suited to this challenge. They occupy an area in which there are strong spatial gradients in both mass balance and the magnitude and seasonality of predicted climate changes [*Maxwell*, 1997], and they will have shorter response times to climate change than the larger Greenland ice sheet. In addition, there is substantial variability in ice dynamics between different basins within the same ice cap. Typically, these ice caps have both terrestrial and tidewater margins, and they may contain fast flowing outlet glaciers, surge-type glaciers and more slowly moving lobate sectors. They can thus be expected to display a diversity of responses to climate change. The main aim of this paper is to determine the contribution of surface mass balance to observed changes in the geometry of a high Arctic ice cap over the last 4 decades.

[3] We use a combination of long-term mass balance field measurements from the accumulation area and degree-day melt model output to present a spatially resolved reconstruction of 37 year average accumulation and ablation rates across the Devon Ice Cap (Figure 1) in the Canadian high Arctic. The contribution of surface mass balance to observed changes in the geometry and volume of the ice cap over the last 4 decades [*Burgess and Sharp*, 2004] is then determined for the ice cap as a whole and for each of the major drainage basins. This research is part of an integrated study of the area/volume change and dynamics of the Canadian Arctic ice caps and will provide the necessary baseline data required to estimate balance fluxes for the ice cap (following *Budd and Warner* [1996]).

2. Field Site

[4] Devon Ice Cap covers ~14,000 km^2 on eastern Devon Island, Nunavut, Canada (Figure 1). It has a maximum elevation of 1930 m above sea level (asl). It is slightly asymmetrical, with an east-west summit ridge, which is more pronounced in the east, and a southern ridge that begins ~20 km south of the summit and extends south to

0148-0227/05/2003JF000099$09.00

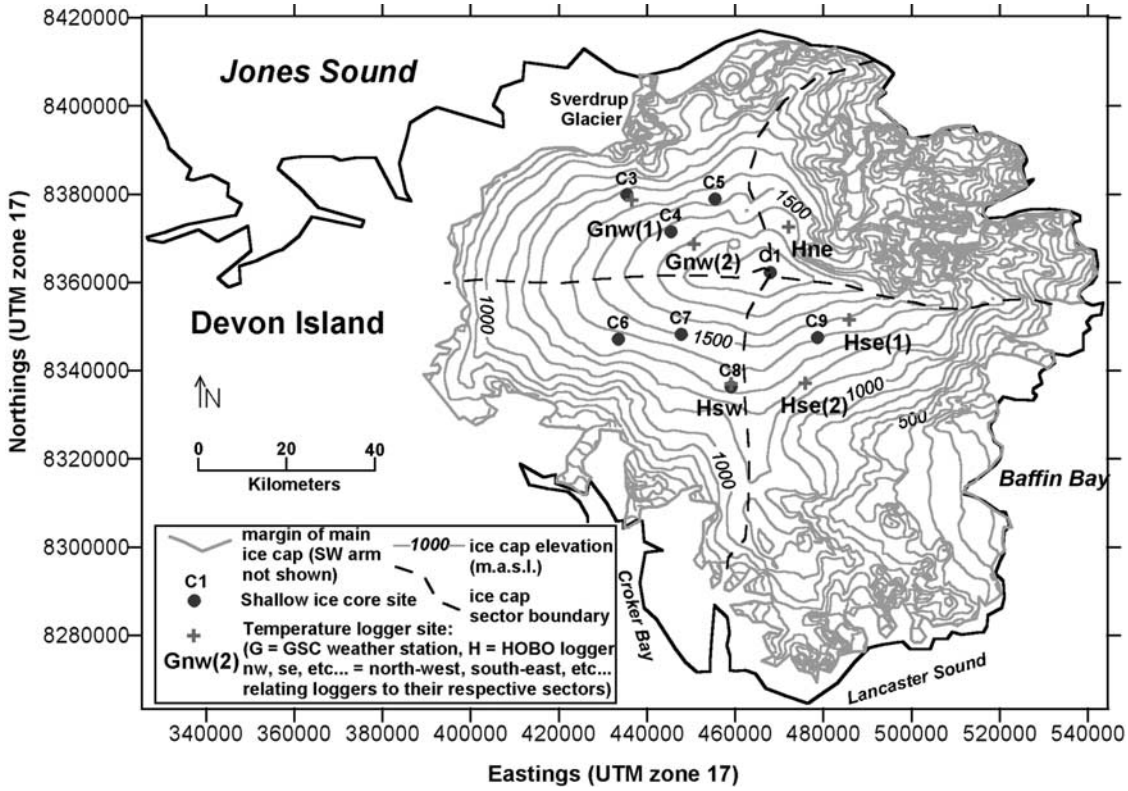

Figure 1. Devon Ice Cap fieldwork locations.

within a few kilometers of Lancaster Sound. The ice cap has been the focus of mass balance measurements since the early 1960s [*Koerner*, 1966, 1970; *Koerner and Taniguchi*, 1976]. Maps of mass accumulation were produced from snow depth measurements along several profiles across the ice cap [*Koerner*, 1966]. An annual mass balance measurement program was conducted along profiles that ran from the summit of the ice cap, northwest along the Sverdrup glacier basin to the coast, and southeast toward Lancaster Sound [*Koerner*, 1970]. In the mid-1970s, longer-term average accumulation rates were estimated from laboratory analyses of two shallow ice cores retrieved from the northwest transect [*Koerner and Taniguchi*, 1976]. The cores were analyzed to detect the radioactive layer deposited in 1963 as a result of H-bomb tests in 1962. Measurements of ice density above this layer allowed estimation of average accumulation between 1963 and 1974. Mass balance monitoring has continued and is ongoing along the northwest transect across Devon Ice Cap [*Dyurgerov*, 2002]. However, repeat measurements of stake arrays on remote ice masses are very time consuming and expensive [*Fountain et al.*, 1999], so no continuous measurements of mass balance have been made across the rest of the ice cap.

3. Methods and Data Acquisition

[5] In this study, a combination of shallow ice core measurements and degree-day modeling is used to map the spatial distribution of average mass balance across the Devon Ice Cap. A combination of methodologies is used because (1) long-term field measurements can effectively constrain the spatial pattern of mass balance across much of the accumulation area, but are not of sufficiently good spatial and temporal coverage to simply carry out a statistical extrapolation of measurements across large ablation areas of the ice cap at lower elevations and (2) simple degree-day melt modeling works fairly well for lower elevations across the ablation area, but struggles with the highly nonlinear snow accumulation/elevation relationship which exists at Devon Ice Cap, particularly within the accumulation area.

3.1. Shallow Ice Coring

[6] During April–May 2000, eight shallow (<20 m) ice cores were drilled across the accumulation area of Devon Ice Cap (Figure 1, C1–C9) using a Kovacs Mark II ice corer. The corer produces cores with diameters of 9 cm and average lengths of ~40 cm. Snow and firn densities were determined immediately after retrieval of cores by measuring the diameter, length and weight of each core section.

[7] Using a down-borehole gamma spectrometer (NaI(Tl)) detector with photomultiplier tube and MicroMCB multichannel analyzer software), gamma activity profiles of each borehole were measured using a method similar to that described by *Dunphy and Dibb* [1994]. Measurements of gamma ray counts accumulated over 1200 s were made for the energy bands of a ^{109}Cd reference source, ^{137}Cs and 2 other spectral intervals. Counts were conducted at 40 cm intervals, working upward from the bottom of each borehole. Profiles for all spectral intervals except ^{109}Cd show an exponential increase toward the surface that is most likely due to cosmic ray–produced gamma rays [*Dunphy and Dibb*, 1994]. The count profiles for ^{137}Cs showed a secondary peak at depth (e.g., Figure 2) that is associated with peak fallout from atmospheric testing of thermonuclear weapons in 1962–1963. Profiling resolution was increased

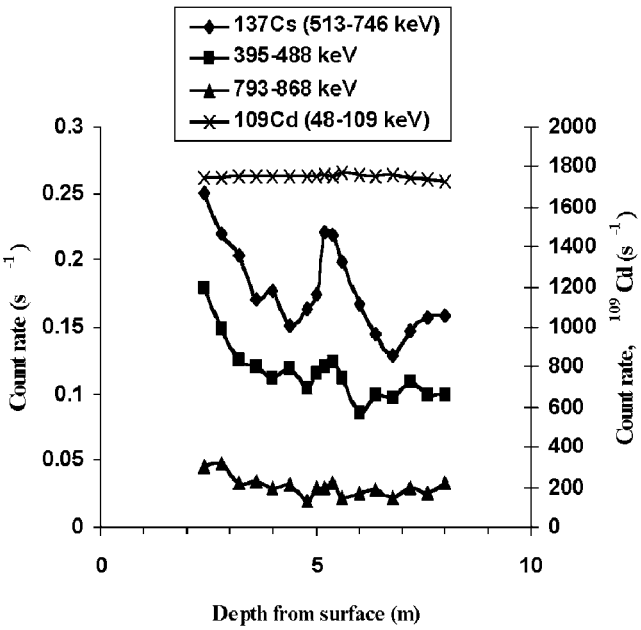

Figure 2. Gamma ray count-depth profiles for four energy ranges at core C3.

to 20 cm intervals around the peak to determine its location more accurately.

[8] Using the depth of the 1963 radioactive fallout layer and measurements of the densities of firn and snow above this layer, the average mass balance over the period 1963–2000 was estimated at each core site in the field. There are errors associated with in situ density profiling. Determining the average density of the core is relatively straightforward at higher elevations (e.g., core 1 at the summit), where coherent sections of relatively low-density firn were retrieved. Closer to the equilibrium line (e.g., core 3), within the "saturation zone," core sections were composed of refrozen slush which frequently broke into more irregularly shaped sections that were more difficult to measure. The error in determining the average density of the entire core was, however, likely reduced by the relatively uniform density and character (e.g., bubble content) of firn from these regions. We estimate that (1) the error in total volume of the core above the bomb layer is ~10%, (2) the error in the weight of the core is ~1%, and (3) the error in the depth of the bomb layer is ~0.5–2%. We therefore estimate that the long-term mass balance at a point can be determined with an accuracy of ~12%.

[9] A more fundamental uncertainty concerns the ability of a measurement based on a single core to represent the average accumulation rate across a larger area. Variations in annual accumulation can occur, for instance due to the formation of sastrugi, over spatial scales of 10^{-2}–10^{2} m. Since we do not know spatial covariance functions for the mean accumulation rates across the ice cap this uncertainty cannot be resolved, although it is likely to be diminished over a period of 37 years.

3.2. Air Temperature Loggers

[10] In May 2000, four 8K HOBO™ temperature loggers were deployed to measure average daily surface air temperature within the northeastern, southeastern and southwestern sectors of the ice cap at elevations of ~1640 m, 1530 m, 1190 m and 1320 m respectively (Figure 1, Hne, Hse(1), etc.). The Geological Survey of Canada (GSC) has deployed automatic weather stations (AWS) and recorded air temperatures at sites within the northwestern sector of the ice cap (two of these are located in Figure 1: Gnw(1) and Gnw(2)) almost continuously during the 1990s and periodically before this, but has no record of air temperatures elsewhere on the ice cap. Data from HOBO loggers and AWSs were downloaded in April 2001 and used to generate input for degree-day melt modeling (see Appendix A).

3.3. Degree-Day Melt Modeling

[11] The daily snow or ice melt at any point is often assumed to be proportional to the daily mean air temperature at that location so long as the mean air temperature is positive. The constant of proportionality between the melt rate and the air temperature is termed the "degree-day factor," and is generally lower for snow (DDF_s) than for ice (DDF_i) [*Braithwaite*, 1995]. This method of estimating ablation has been applied effectively in Greenland [*Braithwaite and Olesen*, 1989; *Huybrechts et al.*, 1991], and to John Evans Glacier, Ellesmere Island [*Arendt and Sharp*, 1999] and several glaciers in the Swiss Alps [*Braithwaite and Zhang*, 2000]. DDF_s and DDF_i are not universal across all ice masses [*Braithwaite and Zhang*, 2000], however, since they depend on the energy balance at each location. Although the method is a crude simplification of the complex processes involved in the surface energy balance, it is very useful for application to areas for which input data are sparse. Using this approach, temporal patterns of melt at a specific glacier can be estimated from measurements at remote stations so long as (1) some measurements of mass balance are available to constrain the degree-day factors for the glacier and (2) there are sufficient temperature data from the glacier to determine a relationship with measurements at the remote station.

4. Results

4.1. Shallow Ice Coring

[12] Depth profiles of density and ^{137}Cs gamma count rates for four sites within the northwest sector of the ice cap are shown in Figure 3. At higher altitudes, firn densities are low at the surface and increase gradually with depth. At lower altitudes the annual accumulation consists of refrozen saturated snow, and firn densities are closer to that of pure ice. The ^{137}Cs profiles each show a distinct peak at depth (peak ~0.25 ^{137}Cs counts s^{-1} compared with a background count rate at depth of ~0.15 ^{137}Cs counts s^{-1}). In the northwest sector of the ice cap the peaks are generally closer to the surface at lower elevations.

[13] At the summit, two gamma profiles were measured; one in a shallow borehole (C1, Figure 3a), and one in a slightly narrower borehole drilled to ~60 m depth by the GSC (C2, Figure 3a). The ^{137}Cs peak appears on both profiles ~18 m from the surface. Assuming that this peak represents the 1963 fallout layer, the average mass balance at the summit for the period 1963–2000 was calculated as 0.241 ± 0.03 meters water equivalent per year (mWe a^{-1}). This compares with values in the range 0.216–0.234 mWe a^{-1} calculated by the GSC based on identification of annual layers

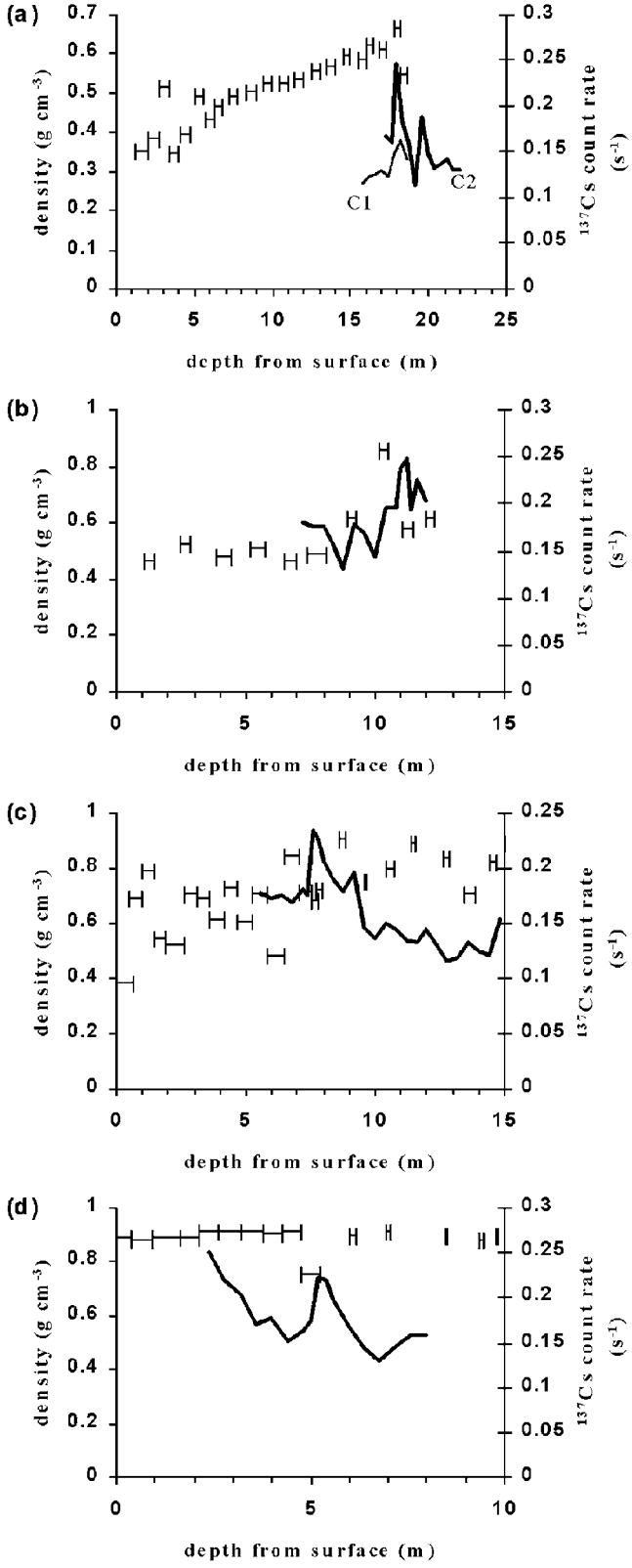

Figure 3. Density and ^{137}Cs count rates: (a) summit cores, C1 and C2 (GSC core), 1930 m asl; (b) C4, 1640 m asl; (c) C5, 1508 m asl; and (d) C3, 1340 m asl.

Table 1. Mass Balance Calculated From Shallow Ice Core Measurements on Devon Ice Cap, April–May 2000[a]

Core Site	Elevation, m asl	Depth of 1963 Layer in 2000, m	Mass Balance 1963–2000, mWe
C1	1930	18.0	0.241
C4	1640	11.2	0.159
C5	1508	7.6	0.138
C3	1340	5.2	0.127
C7	1504	10.2	0.159
C9	1470	10.6	0.218
C6	1367	10.4	0.201
C8	1325	15.2	0.267

[a]C1–C5 are in northern half of ice cap; C6–C9 are in southern half of ice cap.

using major ion concentrations and laboratory density measurements over a range of timescales dating back to the Laki eruption of 1783 [*Pinglot et al.*, 2003]. The consistency between GSC measurements and shallow ice core results gives us confidence that the ^{137}Cs peak at depth clearly represents the 1963 radioactive fallout layer and that the method is successful in determining the long-term, average mass balance.

[14] The 1963 fallout layer was also located at four sites across the southern half of the ice cap (C6–C9, Figure 1; Table 1). Estimates of the long-term average mass balance for all 8 sites, distributed across the accumulation area of the ice cap, are presented in Table 1. Long-term mass balance, estimated from shallow ice cores in the northwest sector of the ice cap, is generally consistent with a range of previous stake measurements from the 1960s and core measurements from 1963–1974 (Figure 4a). Note that there was an exceptionally high level of melt across the ice cap in 1962 [*Koerner*, 1970]. In contrast to the northwest sector of the ice cap, both shallow ice cores and annual mass balance measurements show that there is no clear relationship between mass balance and elevation to the south and east (Figure 4b).

[15] A comparison of the 1963–1974 and 1963–2000 ice core measurements reveals two patterns (Figure 4a). Firstly the better spatial resolution of the 1963–2000 core measurements identifies a slightly nonlinear mass balance-elevation relationship. Mass balance falls rapidly from the summit (1930 m) to ~1600 m and decreases more gradually from there toward ~1300 m. This pattern is likely to reflect the erosive action of katabatic winds, which are most persistent from ~1600 to 1800 m. These winds remove winter snowfall from these altitudes and deposit it at lower elevations [*Koerner*, 1966]. Secondly, there may have been a reduction in the net mass balance since 1974 at lower elevations in the accumulation area (~1300 m), though some of this may be accounted for by errors.

[16] The lack of a clear relationship between mass balance and elevation in the south and southeast sectors of the ice cap probably reflects the strong influence of Baffin Bay on patterns of accumulation in these areas. Northern Baffin Bay remains ice-free for most of the year and cyclones bring moist air across the southern and eastern regions of the ice cap. Most of the moisture is deposited as snow as it reaches the eastern slopes of the cold ice cap [*Koerner*, 1966]. Higher melt at lower altitudes will be balanced by higher accumulation rates nearer Baffin Bay. Net mass balance can

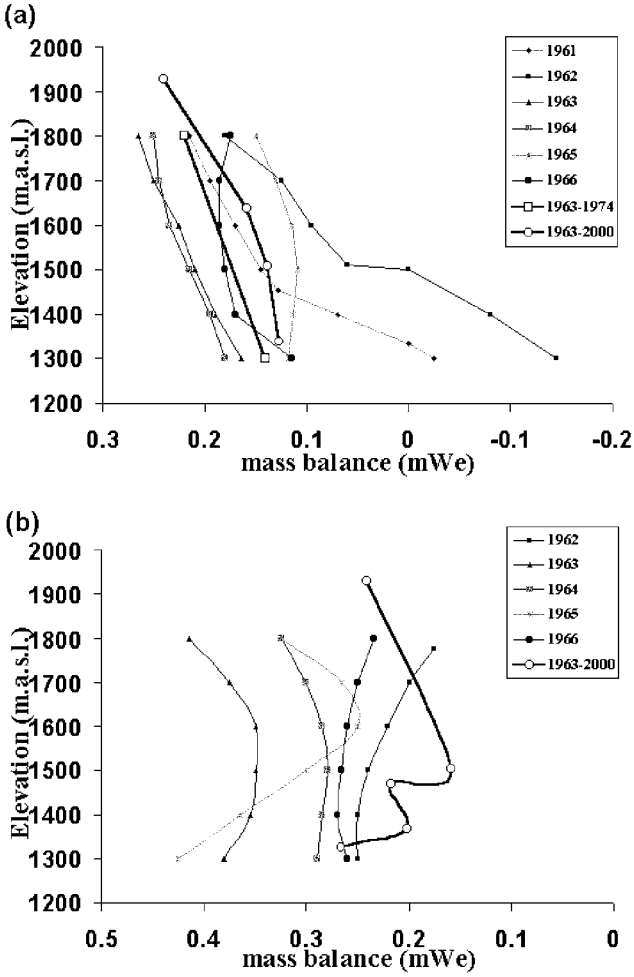

Figure 4. Mass balance from cores over period 1963–2000 compared with annual mass balance measurements from the 1960s [*Koerner*, 1970] and (in Figure 4a) with shallow ice core experiments in 1974 [*Koerner and Taniguchi*, 1976]. (a) Northwest sector accumulation area. (b) South and southeast sectors accumulation areas.

therefore even out at values similar to those measured at higher elevations.

4.2. Degree-Day Modeling: Simulation of Long-Term Temperature Data for Different Sectors of the Ice Cap

[17] Summer melt over the ice cap was simulated using the degree-day model of *Arendt and Sharp* [1999]. For the purposes of degree-day modeling, the ice cap was subdivided into four sectors (Figure 1). Temperature data from different loggers were used to generate input data for modeling melt in each sector. On-ice temperature data for all sectors were gathered for the period May 2000–April 2001 only. Thus to model the mass balance of the ablation zone over a period of ~40 years, it was necessary to determine the relationship between air temperatures on the ice cap and those at the nearest location for which records extend back to the early 1960s (Resolute Bay). For the purposes of degree-day modeling, it is important that the simulated long-term temperature records predict accurately the number of positive degree-days at each temperature logger site.

[18] Linear regression equations were derived to express the relationship between daily average temperatures at Resolute Bay and in each sector of the ice cap for the period day of year 150 (D150) to D250 (May 30 to September 7), 2000 (e.g., Figures 5a and 5b). Surface melt is not expected outside this period. These equations were used to predict temperatures on the ice cap from the Resolute Bay time series. The predicted temperatures (e.g., "predGnw(1)," Figure 5c) seriously underestimate the number of positive degree-days recorded on the ice cap. It is assumed that the difference between predicted and recorded temperature series was due to two factors: (1) different synoptic weather conditions over Resolute Bay and Devon Ice Cap and (2) error induced by the simple linear regression. Synoptic differences are expected to average out over seasonal and multiyear periods. Error in the regression was corrected for as follows. It was assumed that half the difference between each predicted and recorded temperature was due to error in the regression and the rest due to synoptic effects. The time series of half the difference between the predicted and recorded ice cap temperatures for the period D150–250, 2000, was therefore used to create a distribution of error terms. These errors were randomly redistributed and then added to the predicted temperature series for the potential melt period (i.e., D150–250). This process was repeated 37 times for each year from 1963–2000. The resulting time series for the potential melt period of the year 2000 ("corrpredGnw(1)," Figure 5d) has a similar number of positive degree-days to the original temperature time series recorded on the ice cap. The process was repeated for all four sectors of the ice cap, and the resulting simulated 1963–2000 temperature records were used as input to the degree-day model. This method assumes that the error distribution is stationary throughout the study period, an assumption that has not been tested.

4.3. Running the Degree-Day Model

[19] Other input data required to run the model were as follows: (1) altitude of temperature record, derived from differential GPS measurements; (2) surface air temperature lapse rate (the average summer lapse rate (-0.0048°C m^{-1}) was calculated using data from GSC AWSs located at 1930 m, 1730 m, 1340 m and 330m elevations within the northwest sector); (3) accumulation, specified as a multiple, k, of the sum of daily accumulation measured at Resolute, where k is the average winter snow fall at each ice cap sector temperature logger elevation (recorded in May 2000 and 2001) divided by total winter snowfall at Resolute up to the same date; (4) accumulation lapse rate, derived from measurements of snow depth at ice cap temperature loggers and at the ice cap summit (0.00002 mWe m^{-1} for the southwest sector, 0.00005 mWe m^{-1} for the other 3 sectors); (5) maximum amount of superimposed ice formed during the melt season, calculated using the temperature method [*Woodward et al.*, 1997], which requires the mean annual sea level temperature for Devon Island (-13.6°C). This was extrapolated from the linear relationship between annual average air temperatures and elevation determined using data from GSC AWS.

[20] A potentially significant limitation of the melt model is that temperature and accumulation lapse rates are taken as constants when there is field evidence which suggests they

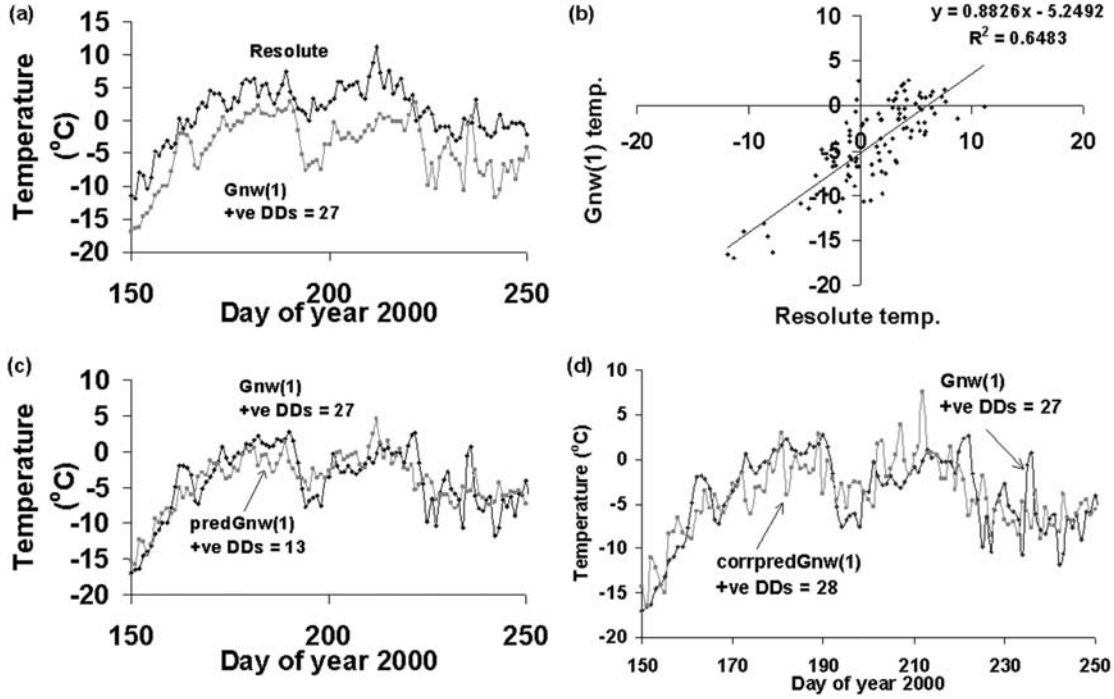

Figure 5. Stages in the simulation of daily average temperatures for the northwest sector of the ice cap from Resolute Bay temperature data. (a) Daily average temperatures at Resolute Bay and at AWS Gnw(1) over period D150–250, 2000. (b) Linear regression relationship between Resolute Bay and Gnw(1) temperature data over same period. (c) Gnw(1) data compared with predicted temperature data (predGnw(1)) from linear regression with Resolute Bay data. (d) Gnw(1) data compared with corrected, predicted temperature data (corrpredGnw(1)) after random redistribution of error terms.

are not. The average temperature lapse rate calculated from AWS measurements along the northwest transect, masks frequent temperature inversions and is likely to be very dependent on variations in katabatic winds [*Denby and Greuell*, 2000]. The effect of inversions and katabatic winds will be particularly significant when they occur during the summer when temperatures approach 0°C. Winter accumulation patterns across Devon Ice Cap do not show a linear decrease with altitude. According to *Koerner* [1966], accumulation actually reaches a maximum around the equilibrium line in the southeast sector. Although the melt model is primarily used to estimate mass balance in the ablation areas of the ice cap, accumulation lapse rates were calculated from measurements made in the accumulation area only. A more general limitation of the melt model is that a considerable amount of empirical data is needed to calibrate and/or constrain model output. Devon Ice Cap is a good place to apply such a model because of the existence of field measurements of mass balance across different sectors of the accumulation and ablation areas. Where fewer empirical data are available to constrain model output, the selection of degree-day factors will be even more subjective.

4.4. Model Tuning

[21] Since previous research (summarized by *Braithwaite and Zhang* [2000, Table 4]) has shown that no unique set of DDFs can be applied to all ice masses, DDF_s and DDF_i must be assumed to be unknown. The following steps were followed to determine the most appropriate DDFs for each sector of the ice cap.

[22] 1. The melt model was run for the periods for which stake measurements of annual mass balance exist at 100 m altitude intervals: 1961–1966 in the northwest sector; 1962–1966 in the southeast sector.

[23] 2. For each of these sectors the model was run forty times with different sets of DDFs for snow and ice: DDF_s was varied between 2.5 and 4 mm d^{-1} $°C^{-1}$ with an interval of 0.5; DDF_i was varied between 5 and 14 mm d^{-1} $°C^{-1}$ with an interval of 1. These values cover the typical range of DDFs for Arctic and Alpine glaciers (summarized by *Braithwaite and Zhang* [2000, Table 4]).

[24] 3. The accuracy of each model run was expressed by the error, e, between the mean values of modeled and measured mass balance at the jth altitude, b_j^* and b_j respectively, such that

$$e = \sqrt{\left(1/J \sum_{j=1}^{j=J} \left(\left(b_j^* - b_j\right)/2\right)^2\right)}, \quad (1)$$

where J is the number of elevation intervals. Thus e is the square root of the mean of the squares (rms) of half of the differences between measured and modeled values.

[25] 4. The DDFs from the best fit model runs were used with the simulated 1963–2000 temperature data to calculate long-term mass balance for the northwest and southeast sectors.

[26] 5. In the absence of stake or core measurements for the northeast sector, best fit DDFs from the northwest sector were applied to simulated temperature data for the adjacent

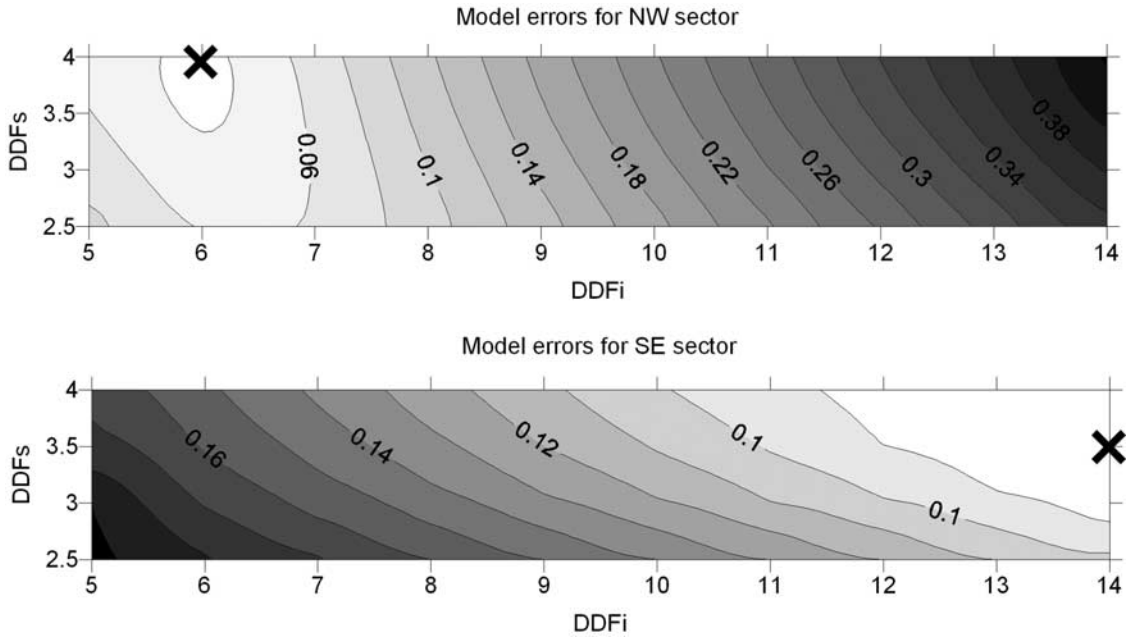

Figure 6. Model errors for northwest and southeast sectors. Lowest errors are run 32 for the northwest sector and run 30 for the southeast sector.

northeast sector. Since core measurements from the southwest sector and stake measurements from the southeast sector both display a nonlinear relationship between mass balance and elevation (Figure 4b), it was assumed that best fit DDFs from the southeast sector could be applied to simulated temperature data for the southwest sector.

[27] The areas of each elevation interval were not factored into equation (1) since, unlike well-defined valley glacier catchments, these are highly dependent upon the fairly arbitrary nature of the sector boundaries. This could lead to the undesirable situation where the most appropriate DDFs for each sector may become as dependent on the exact locations of the sector boundaries as on the comparison with measured data. The model errors and DDF ranges for each model run are shown for the northwest and southeast sectors in Figure 6. A number of model runs give low errors. The best fit values for the northwest sector are $DDF_s = 4$ mm d^{-1} $°C^{-1}$ and $DDF_i = 6$ mm d^{-1} $°C^{-1}$ (model run 32); and for the southeast sector, $DDF_s = 3.5$ mm d^{-1} $°C^{-1}$ and $DDF_i = 14$ mm d^{-1} $°C^{-1}$ (model run 30). These DDFs lie within the range of values used previously [*Braithwaite and Zhang*, 2000, Table 4]. The differences in these DDFs for different sectors should not be physically interpreted since these are sensitive to varying winter accumulation which, as mentioned above, is not well constrained by linear lapse rates. Despite this, modeled mass balance compares favorably with the limited number of shallow ice core measurements averaged over the period 1963–2000 in the northwest, southeast and southwest sectors and with 1960s stake measurements (Figure 7). No long-term data exist for the northeast sector.

4.5. Combining Modeled and Measured Mass Balance

[28] For each sector of the ice cap, high-order polynomial regression trend lines were fitted to plots of modeled mass balance against elevation. The regression equations were used to predict the mass balance distribution across the ice cap with 1km spatial resolution using 1 km digital elevation models (DEMs) of each sector.

[29] Shallow ice coring experiments provide long-term measurements of mass balance, and are assumed to be more accurate and reliable than modeled mass balance. Therefore across most of the accumulation area, mass balance was interpolated from the distribution of core measurements (using a 1 km grid block kriging routine) and then combined with modeled mass balance associated with the remainder of the ice cap. This was carried out as follows.

[30] Net accumulation in the west of the ice cap is well constrained by core measurements from an ice cap summit value of 0.241 mWe a^{-1} to 0.127 mWe a^{-1} at C3 (Figure 1). Melt model output for the western half of the ice cap was therefore only used to predict mass balance across those areas where modeled values were less than 0.1 mWe a^{-1}. Accumulation in the east is less well constrained by measurements (0.241 mWe a^{-1} at summit to 0.217 mWe a^{-1} at C9), so modeled mass balance values less than 0.15 mWe a^{-1} were retained. By choosing this higher value, model output is used to predict mass balance across inaccessible mountainous areas in the northeast and southeast that show evidence of accumulation (e.g., extensive areas of ice-covered summits). A 1 km grid of surface mass balance across the entire ice cap was therefore created from merging five grids; the shallow ice core-constrained grid, covering most of the accumulation area, and melt model grids from each of the four sectors covering the remainder of the accumulation area and ablation area. A contour map of mass balance was created from these merged grids using the Golden Software, Inc. ''Surfer'' program (Figure 8). The error distribution across the ice cap was calculated by assuming an error of 12% in the core measurements, and using equation (1) to estimate errors averaged across different sectors of the rest of the ice cap (inset of Figure 8).

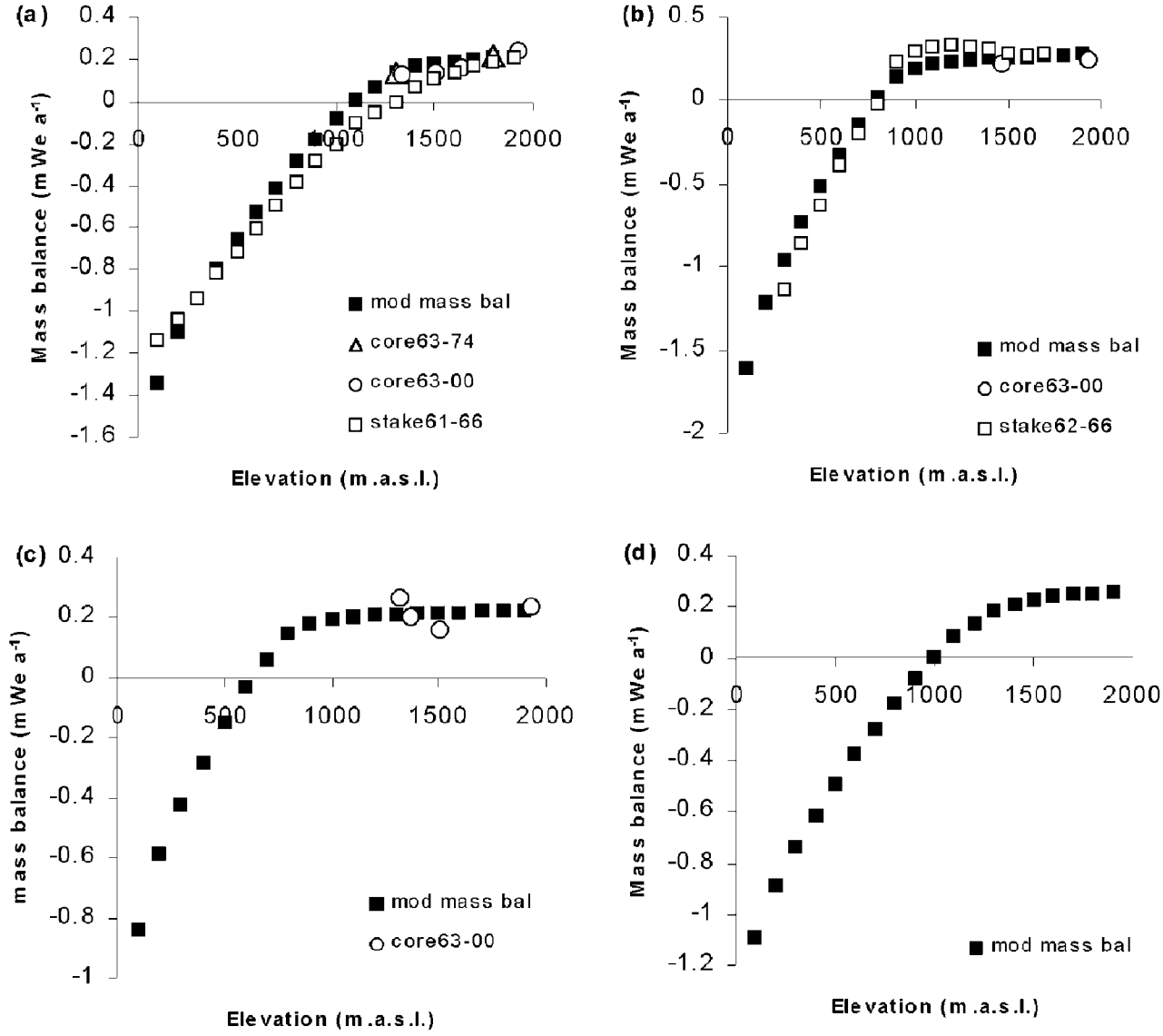

Figure 7. Modeled mass balance, shallow ice core and stake measurements of mass balance for different sectors of Devon Ice Cap. (a) Northwest sector. (b) Southeast sector. (c) Southwest sector. (d) Northeast sector.

4.6. Contribution of Surface Mass Balance to Volume Change of Devon Ice Cap

[31] The contribution of surface mass balance to observed changes in volume of the ice cap can now be estimated by calculating the net "volume" of the mass balance grid upon which Figure 8 is based. This was done using the "Surfer" Grid/Volume function that calculates the net volume between a grid surface and a horizontal plane, which, in this case, is where mass balance equals zero. Three methods were used to determine volumes: Extended Trapezoidal Rule, Extended Simpson's Rule, and Extended Simpson's 3/8 Rule [*Press et al.*, 1988, section 4.1]. The difference in the volume calculations by the three different methods measures the accuracy of the volume calculations. In all cases the volume calculations were very close (within 0.005 km^3 We a^{-1}), so an average of the three values was taken.

[32] The northwest sector of the ice cap (Figure 1) has lost 6.4 ± 3 km^3 water over the period 1963–2000. This equates to an average surface mass balance of -0.067 ± 0.03 mWe a^{-1} which compares with the value of -0.049 mWe a^{-1} calculated based on repeat annual mass balance stake measurements over the period 1963–1998 in this region (measured by Koerner, quoted by *Dyurgerov* [2002]). The main part of Devon Ice Cap (i.e., excluding the southwest arm) has lost 59.2 ± 26.6 km^3 (or 1.6 ± 0.7 km^3 a^{-1}) over the period 1963–2000. This equates to an average surface mass balance (SMB) of -0.13 ± 0.056 mWe a^{-1}. This result can be compared with completely independent volume change estimates for a similar time period, which we now summarize.

[33] *Burgess and Sharp* [2004] calculated volume change of the Devon Ice Cap over a 40 year period using two independent methods based on areal changes measured from 1959/1960 aerial photography and 1999/2000 Landsat 7 ETM+ satellite imagery. The first method estimates the

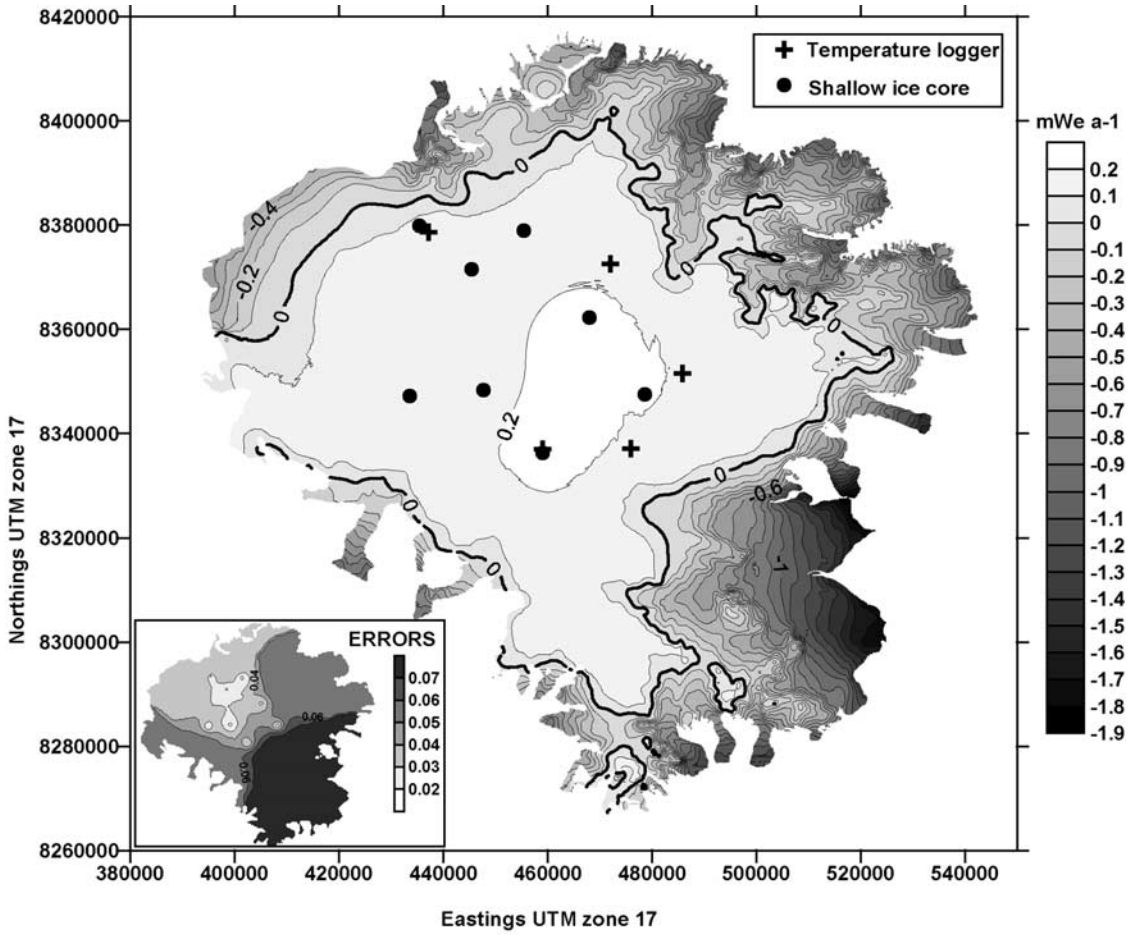

Figure 8. Spatial pattern of mass balance determined from combination of shallow ice core measurements and degree-day melt model output (units of mass balance in mWe a^{-1}). Equilibrium line highlighted.

change in cross sectional area of a longitudinal profile of a glacier as the product of the maximum glacier thickness (MT) and the length change at the terminus [*Hooke*, 1998, p. 219]. However, to account for glacier width, the total area change (instead of the length change alone) calculated for each individual drainage basin (Figure 9), was multiplied by the maximum ice thickness within the associated catchment area (obtained from recent radio echo sounding (RES) data collected by J. Dowdeswell, Cambridge University, UK, 2000). Volume change measurements were calculated over 86% of the ice cap area and extrapolated over the remaining 14% indicating a total volume change of 44 ± 9 km^3 (excluding the southwest arm), or 1.1 km^3 per year over the period 1960–1999. The second method used volume-area (VA) scaling techniques [*Bahr et al.*, 1997], and estimated volume change for the main portion of the ice cap as 52 ± 5 km^3. Given the large scope for measurement and methodological errors, the three different methods (SMB, MT and VA) give comparable total volume loss estimates for Devon Ice Cap over approximately the last 4 decades.

5. Analysis and Discussion of Spatial Variations in Mass Balance and Volume Change

[34] *Burgess and Sharp* [2004] identified significant spatial changes in the geometry of Devon Ice Cap since 1960. These included (1) the retreat of major tidewater glaciers along the east coast, (2) an increase in exposed bedrock area in mountainous northeast and southeast regions, indicating lowering of the ice cap surface, (3) an ice margin advance of ~130 m along an 80 km section of the northwest margin, and (4) minor marginal advance of smaller glaciers in the northwest (Sverdrup Glacier) and south of the ice cap (Croker Bay glacier catchments). In order to determine the contribution of SMB to these changes, we compared SMB estimates of volume change with estimates using the MT method described above for each of the largest major drainage basins (17 basins, excluding the southwest arm (Figure 9)). Volume change estimates derived from the MT method were used for the comparison because this method allowed volume changes to be calculated for individual drainage basins whereas volume change estimates derived from the volume-area scaling technique were calculated for the ice cap as a whole only. SMB estimates are extrapolated over a 39 year period in order to facilitate comparison with volume change estimates derived from the MT method.

[35] The relationship between the MT and SMB estimates of volume change (over the 17 basins for which the MT method was used) is quite strong (Figure 10a, $r^2 = 0.68$). There is no significant relationship between the area of each

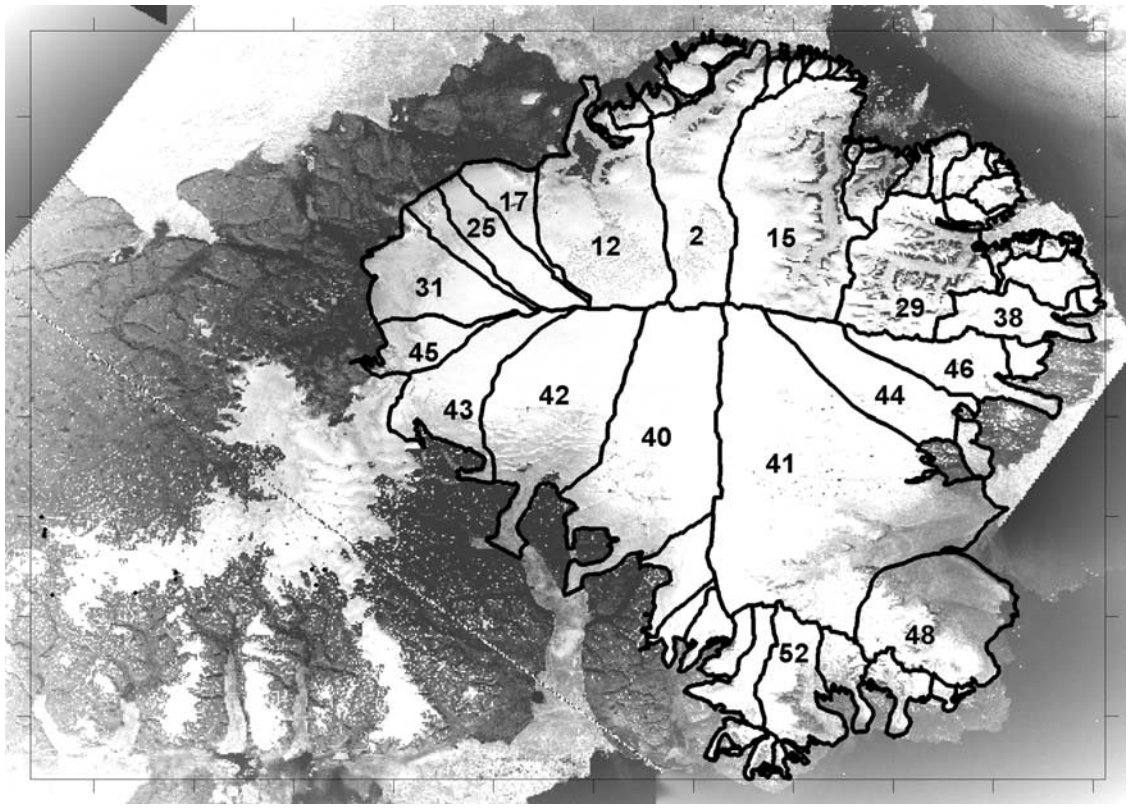

Figure 9. Drainage basins of the Devon Ice Cap. The southwest arm was not included in this analysis.

drainage basin and the difference between these two estimates of volume change. The largest 17 basins account for 86% of the area of the ice cap (excluding the southwest arm) but only ~68% of the total volume loss estimated from SMB measurements. The remaining 14% of the ice cap accounts for ~32% of mass loss due to SMB. Thus the small basins may make a disproportionately high contribution to the overall mass loss. This makes physical sense. These basins are found near the ice cap margins, particularly in the southern and eastern sectors, and do not extend to the high interior elevations that the larger basins reach. They have much larger ablation areas in proportion to the total

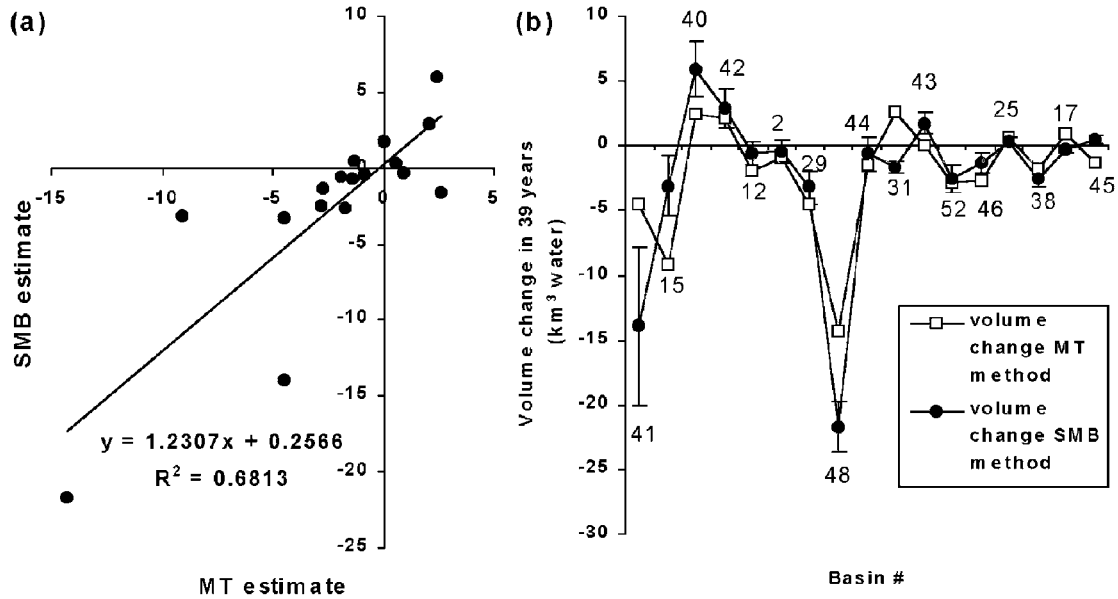

Figure 10. Surface mass balance (SMB) estimate of volume change extrapolated over 39 years and compared with maximum thickness (MT) estimate. (a) Linear regression relationship between SMB and MT volume change estimates. (b) Individual basin comparison (with error bars on SMB estimate).

basin area (lower accumulation area ratios). Preferential thinning of up to 10 cm a^{-1} was detected from repeat airborne laser altimetry profiles flown by NASA in 1995 and 2000 [*Abdalati et al.*, 2005] at two locations along the northwest and southwest margins. This also indicates relatively high rates of ablation at lower elevations of the ice cap. The linear extrapolation of the MT volume change estimates from the largest basins (86% ice cap area) across the rest of the ice cap (i.e., across the smaller basins) will therefore be likely to underestimate the total ice cap mass loss.

[36] A basin by basin comparison of SMB and MT estimates of total mass change over a 39 year period (Figure 10b) identifies very similar patterns of spatial variation in volume change across the largest drainage basins of the ice cap. These are (1) volume loss across many easterly basins (e.g., basins 15, 29, 38, 46, 41, 48, and 52); (2) very little change across much of the western half of the ice cap (e.g., basins 2, 12, 17, 25, 43, and 45); and (3) significant volume increase in southern glacier basins flowing into Croker Bay (i.e., basins 40 and 42).

[37] There are, however, differences between the two sets of estimates that are now discussed further. For eight basins, differences between SMB and MT volume change estimates can be accounted for by errors in the SMB estimate (basins 42, 12, 2, 29, 44, 52, 25, and 38). Other differences could be due to the possibility that the true volume change differs from that determined from the area change, calculated as part of the MT method. If there has been a significant change in the maximum thickness of a basin this will affect the accuracy of the MT estimate of volume change. Figure 10b suggests that highly negative SMB across basins 41 and 48 in the southeast sector should have lead to much greater values of volume loss than estimated by the MT method. The discrepancy could be due to thinning of the ice in these basins which has not been accounted for in the MT method. *Burgess and Sharp* [2004] identified an increase in the area of exposed bedrock in interior regions of the southeast sector of the ice cap, indicating surface lowering of the ice cap over the period 1960–2000. Thus given the error in the SMB estimates and the unknown error in ice thickness used in the MT method, it is likely that SMB can account for mass loss across 10 (65%) of the 17 largest drainage basins.

[38] SMB across basin 31 in the northwest sector suggests this basin has experienced an overall negative balance in recent decades despite the fact that its margin has advanced 130 m between 1960 and 2000. It may be that the maximum ice thickness of this basin has decreased and that marginal advance is a delayed response to a period of positive mass balance at some time in the past. *Burgess and Sharp* [2004] calculated response times of each drainage basin following the method of *Johannesson et al.* [1989] and found that basin 31 has a response time of 677 years. *Burgess and Sharp* [2004, p. 270] came to the conclusion that the advance of the northwest margin "suggests either that conditions favorable to ice sheet growth are prevalent in this region, or that this sector of the ice cap is still responding to the cooler conditions of the Little Ice Age." From the SMB evidence presented here, it would appear that the latter explanation is more likely.

[39] The MT and SMB volume change estimates for the remaining six basins (15, 40, 43, 46, 17, and 45) are -4.6 km^3 and $+3.5$ km^3 respectively. Most of this difference of 8.1 km^3 can be attributed to basin 15. It is likely that iceberg calving accounts for the difference in volume change estimate for this basin where tidewater glaciers have retreated up to 1300 m from 1960 to 2000 [*Burgess and Sharp*, 2004] and where imagery shows the highest concentrations of icebergs in coastal waters.

6. Summary and Conclusions

[40] The spatial pattern of mass balance across Devon Island Ice Cap was reconstructed from two data sources. These were (1) shallow ice core measurements of net mass balance in the accumulation area since the deposition of the 1963 radioactive H-bomb test layer and (2) output (predicted net mass balance) from degree-day melt modeling driven by simulated long-term daily average air temperatures and snow accumulation. Despite potentially significant sources of error, results compared well with previous mass balance measurements from stakes and ice cores. We estimate that Devon Ice Cap (excluding the southwest arm) has lost an average of 1.6 ± 0.7 km^3 water per year over the period 1963–2000. Although the estimated margin of error is large, this estimate compares favorably with completely independent volume change estimates over a similar time period based on measured area changes [*Burgess and Sharp*, 2004]. The contribution of mass balance to recent changes in ice cap geometry was investigated across the largest individual ice drainage basins by comparing mass balance estimates of volume change with estimates based upon measurements of maximum ice thickness and area change. The spatial patterns of mass change across these basins were similar for both sets of estimates. The comparison suggests that surface mass balance is the main cause of volume change. Where differences between the estimates were more significant, these could largely be explained by recognizing that (1) the relationship between volume and area of drainage basins may change through time, so the MT estimates of volume change are incorrect for such cases, that (2) the response times of some drainage basins may be such that recently observed changes in basin area are not a consequence of the recent mass balance regime, and (3) the exclusion of the component of mass loss due to iceberg calving.

[41] This research will provide important input data for balance flux and coupled mass balance dynamics modeling of high Arctic ice caps, and a baseline data set against which to compare future measurements of mass balance to detect evidence for spatial and temporal change.

Appendix A

[42] HOBOs were not placed within mini-radiation covers. This did lead to days of inflated air temperatures due to insulation. The nonshielded HOBO data was compared with a properly shielded AWS data set, where these were at the most similar elevation and location, i.e., Gnw(2) and Hne, located at 1731 m asl and 1637 m asl, respectively (Figure 1). It was realized that HOBO data could be used to derive a good estimate of the temperature over the ice

cap. The best relationship between AWS and HOBO data was obtained if HOBO daily minima were used on days when HOBO daily maxima exceeded 0°C ($r^2 = 0.76$ for the potential melt period JD150–250, $r^2 = 0.967$ for the entire year) instead of always using the HOBO daily average ($r^2 = 0.67$ for JD150–250). Average summer (i.e., D150–250) temperatures of this HOBO derived data were 0.9°C higher than AWS data. About half of this difference could be accounted for by the average lapse rate over the same period (calculated from four GSC AWSs from 1930 m to 330 m as 0.0048°C m^{-1}). The same daily minimum criterion was applied to each HOBO logger data set and the derived data were used to form regression relationships with the Resolute Bay temperature time series. It was decided that this routine was preferable to rejecting all the HOBO data on the basis that they were not properly shielded. This method is likely to overestimate the average temperatures across the ice cap, however this will be a systematic error that subsequent tuning of the model will account for by producing DDFs with lower values.

[43] HOBO loggers were deployed ~1.0 m above snow surface. Difference in height between deployment and downloading varied between 20 cm and 40 cm. All HOBO loggers were closer to the surface when retrieved. Monitoring height above snow surface is usually done using ultrasonic depth gauges (UDGs). UDG data from GSC AWSs have often proved unreliable due to problems with excessive rime ice buildup around sensors (R. M. Koerner, personal communication, 2000). However, summit (1930 m) records show a maximum variation in height of ~50 cm and annual difference (D114 2000 to D113 2001) of ~40 cm. The variation in height of the logger above the snow surface during the potential melt period (D150–250) was just 20 cm. At 1340 m maximum change in height is ~40 cm, annual difference is just 10 cm and from D150–250 the height change was 25 cm. Our measurements of HOBO annual height changes are consistent with changes in height of this magnitude. The literature on vertical gradients in air temperature over melting glaciers usually concentrates on larger-scale variations using vertical profile data from high AWS masts and/or balloons. The literature is dominated by work from Alpine glaciers or Iceland [e.g., *Oerlemans et al.*, 1999; *Denby and Greuell*, 2000; *Greuell and Smeets*, 2001]. At Pasterze, Austria, *Denby and Greuell* [2000] recorded temperatures at a range of heights including 1.0 m and 0.7 m, comparable to the heights of our HOBO loggers. A graph of average temperature over a 2 day fair weather period shows a difference of about 0.5°C between 1.0 m and 0.7 m [*Denby and Greuell*, 2000, Figure 1b]. Vertical temperature gradients are likely to be smaller over a high Arctic polar ice cap than over this warm temperate glacier, but we are unaware of any empirical study of high-resolution, near-surface temperature variations over melting surfaces of much higher latitude ice masses. However, if we take this (probably high) value from the literature we can estimate by how much this error would cause us to underestimate the total PDDs. In the northwest sector of the ice cap (where we use AWS data rather than HOBO data) the PDD total for 2000–2001 was 27.13. If we assume that the height varied linearly during the melt season (D150–250) from 0 to 30 cm, and equate this to a temperature error from 0°–0.5°C, then the PDD total would rise to 32.48, i.e., about a 20% increase. This systematic error will be accounted for by subsequent tuning of the model by producing DDFs with higher values (for the HOBO temp records it will to some extent cancel out the logger shielding error discussed above).

[44] **Acknowledgments.** We thank Roy Koerner, Mike Demuth, and Chris Zdanowicz, National Glaciology Program-Environment Canada/Natural Resources Canada for their logistical support and AWS data, the Leverhulme Trust for a Research Fellowship to D.M., NSERC for an Industrial Postgraduate Scholarship (IPS) to D.B. and for Discovery and equipment grants to M.S., Land Data Technologies (Edmonton), sponsor of an IPS Scholarship to D.B., Canadian Space Agency, Meteorological Service of Canada-CRYSYS, Canadian Circumpolar Institute, and Polar Continental Shelf Project for funding and logistical support, and the Meteorological Service of Canada for providing Resolute meteorological data through the CRYSYS program. We thank the Nunavut Research Institute and the communities of Grise Fjord and Resolute Bay for permission to work on Devon Island. This paper is PCSP contribution number 01603.

References

Abdalati, W., W. Krabill, E. Frederick, S. Manizade, C. Martin, J. Sonntag, R. Swift, R. Thomas, J. Yungel, and R. Koerner (2005), Elevation changes of ice caps in the Canadian Arctic Archipelago, *J. Geophys. Res.*, *110*, F04007, doi:10.1029/2003JF000045.

Arendt, A., and M. Sharp (1999), Energy balance measurements on a high Arctic glacier and their implications for mass balance modelling, *IAHS Publ.*, *256*, 165–172.

Bahr, D. B., M. F. Meier, and S. D. Peckham (1997), The physical basis of glacier volume-area scaling, *J. Geophys. Res.*, *102*, 355–362.

Braithwaite, R. J. (1995), Positive degree-day factors for ablation on the Greenland ice sheet studied by energy-balance modelling, *J. Glaciol.*, *41*, 153–160.

Braithwaite, R. J., and O. B. Olesen (1989), Calculation of glacier ablation from air temperature, West Greenland, in *Glacier Fluctuations and Climate Change*, edited by J. Oerlemans, pp. 219–233, Springer, New York.

Braithwaite, R. J., and Y. Zhang (2000), Sensitivity of mass balance of five Swiss glaciers to temperature changes assessed by tuning a degree-day model, *J. Glaciol.*, *46*, 7–14.

Budd, W. F., and R. C. Warner (1996), A computer scheme for rapid calculations of balance-flux distributions, *Ann. Glaciol.*, *23*, 21–27.

Burgess, D. O., and M. J. Sharp (2004), Recent changes in areal extent of the Devon Ice Cap, Nunavut, Canada, *AAAR*, *36*, 261–271.

Denby, B., and W. Greuell (2000), The use of bulk and profile methods for determining surface heat fluxes in the presence of glacier winds, *J. Glaciol.*, *46*, 445–452.

Dowdeswell, J. A., et al. (1997), The mass balance of circum-Arctic glaciers and recent climate change, *Quat. Res.*, *48*, 1–14.

Dunphy, P. P., and J. E. Dibb (1994), ^{137}Cs gamma-ray detection at Summit, Greenland, *J. Glaciol.*, *40*, 87–92.

Dyurgerov, M. (2002), Glacier mass balance and regime: Data of measurements and analysis, *Occas. Pap. 55*, Inst. of Arct. and Appl. Res. Univ. of Colo., Boulder.

Fountain, A. G., P. Jansson, G. Kaser, and M. Dyurgerov (1999), Summary of the workshop on methods of mass balance measurements and modelling, Tarfala, Sweden, August 10–12, 1998, *Geogr. Ann.*, *81A*, 461–465.

Greuell, W., and P. Smeets (2001), Variations with elevation in the surface energy balance on the Pasterze (Austria), *J. Geophys. Res.*, *106*, 31,717–31,727.

Hooke, L. R. (1998), *Principles of Glacier Mechanics*, 248 pp., Prentice Hall, Upper Saddle River, N. J.

Huybrechts, P., A. Letreguilly, and N. Reeh (1991), The Greenland ice sheet and greenhouse warming, *Palaeogeogr. Palaeoclimatol. Palaeoecol.*, *89*, 399–412.

Intergovernmental Panel on Climate Change (2001), *Climate Change 2001: Impacts, Adaptation, and Vulnerability*, edited by J. J. McCarthy et al., Cambridge Univ. Press, New York.

Johannesson, T., C. F. Raymond, and E. D. Waddington (1989), A simple method for determining the response time of glaciers, in *Glacier Fluctuations and Climate Change*, edited by J. Oerlemans, pp. 343–352, Springer, New York.

Koerner, R. M. (1966), Accumulation on the Devon Island Ice Cap, Northwest Territories, Canada, *J. Glaciol.*, *6*, 383–392.

Koerner, R. M. (1970), The mass balance of Devon Island Ice Cap Northwest Territories, Canada, 1961–1966, *J. Glaciol.*, *9*, 325–336.

Koerner, R. M., and H. Taniguchi (1976), Artificial radioactivity layers in the Devon Island Ice Cap, Northwest Territories, *Can. J. Earth Sci.*, *13*, 1251–1255.

Maxwell, B. (1997), *Responding to Global Climate Change in Canada's Arctic*, vol. 2, *The Canada Country Study: Climate Impacts and Adaptation*, 82 pp., Environ. Can., Downsview, Ont., Canada.

Mitchell, J. F. B., T. C. Johns, J. M. Gregory, and S. F. B. Tett (1995), Climate response to increasing levels of greenhouse gases and sulphate aerosols, *Nature*, *376*, 501–504.

Oerlemans, J., H. Bjornsson, M. Kuhn, F. Obleiter, F. Obleiter, F. Palsson, C. J. J. P. Smeets, H. F. Vugts, and J. De Wolde (1999), Glacio-meteorological investigations on Vatnajokull, Iceland, summer 1996, *Boundary Layer Meteorol.*, *92*, 3–26.

Paterson, W. S. B., and N. Reeh (2001), Thinning of the ice sheet in northwest Greenland over the past forty years, *Nature*, *414*, 60–62.

Pinglot, J. F., et al. (2003), Ice cores from Arctic sub-polar glaciers: Chronology and post-depositional process deduced from radioactivity measurements, *J. Glaciol.*, *49*, 149–158.

Press, W. H., B. P. Flannery, S. A. Teukolsky, and W. T. Vetterling (1988), *Numerical Recipes in C*, Cambridge Univ. Press, New York.

Woodward, J., M. Sharp, and A. Arendt (1997), The effect of superimposed ice formation on the sensitivity of glacier mass balance to climate change, *Ann. Glaciol.*, *24*, 186–190.

D. Burgess and M. Sharp, Department of Earth and Atmospheric Sciences, University of Alberta, Edmonton, Alberta, Canada T6G 2E3. (dob@ualberta.ca; martin.sharp@ualberta.ca)

D. Mair, Department of Geography and Environment, University of Aberdeen, Elphinstone Road, Aberdeen, AB24 3UF, UK. (d.mair@abdn.ac.uk)